

# Learning Data-Driven Stable Koopman Operators

Giorgos Mamakoukas, Ian Abraham, and Todd D. Murphey

Department of Mechanical Engineering, Northwestern University, Evanston, Illinois 60208, USA

[giorgosmamakoukas@u.northwestern.edu](mailto:giorgosmamakoukas@u.northwestern.edu)

**Abstract**—In this paper, we consider the problem of improving the long-term accuracy of data-driven approximations of Koopman operators, which are infinite-dimensional linear representations of general nonlinear systems, by bounding the eigenvalues of the linear operator. We derive a formula for the global error of general Koopman representations and motivate imposing stability constraints on the data-driven model to improve the approximation of nonlinear systems over a longer horizon. In addition, constraints on admissible basis functions for a stable Koopman operator are presented, as well as conditions for constructing a Lyapunov function for nonlinear systems. The modified linear representation is the nearest *stable* (all eigenvalues are equal or less than 1) matrix solution to a least-squares minimization and bounds the prediction of the system response. We demonstrate the benefit of stable Koopman operators in prediction and control performance using the systems of a pendulum, a hopper, and a quadrotor.

## I. INTRODUCTION

### A. Challenges in Robotics

Uncertainty in robotic applications can cause failure due to poor prediction and control. The dynamics of robots can be unknown or stochastic (e.g. Sphero SPRK [1], soft robotics [2], [3]) and environments that are complex and ever changing, such as sand [4]–[6] or water [7]–[10], are hard to model accurately. To predict and control systems with unknown or uncertain dynamics, system identification methods are used to develop or adapt a model from data [11]–[16]. To improve the learning rate and the quality of the identified dynamics, active learning methods strategically maneuver a robot to collect measurements that will reduce the uncertainty of the dynamics and the environment [17]–[20]. However, even when dynamics are accurately learned or updated, real-time control of many systems often remains challenging due to the high nonlinearity typically present in robotics [21].

### B. Benefits and Applications of Koopman Operators

To address the uncertainty and nonlinearity of dynamics, recent efforts have focused on data-driven methods that compute linear embeddings of nonlinear systems. The Koopman operator [22] linearly evolves functions of states [23]–[26] and has gained attention for the purposes of both system identification [27] and real-time control of nonlinear systems [26]. Besides simplicity, using the Koopman linear representation for control can in certain cases also outperform feedback policies that are based on the underlying nonlinear dynamics [28], [29]. However, unless finite-dimensional Koopman invariant subspaces exist [28], [30], [31], the operator is infinite-dimensional and renders practical use challenging. Studies seek finite-dimensional approximations using methods such

as the Dynamic Mode Decomposition (DMD) [32] extended DMD (EDMD) [33], [34], Hankel-DMD [35], or closed-form solutions [36], [37] which use state measurements to approximate Koopman operators. Data-driven Koopman operators have already been used in many applications, such as robotics [1], [2], [38], human locomotion [39], neuroscience [40], fluid mechanics [41], and climate forecast [42]. Contrary to linearization methods that remain locally accurate and are often updated online increasing the computational workload, in most cases researchers seek Koopman representations that are calculated once [2]. When the Koopman representation is not updated, for reasons such as limited memory and computational power or even lack of closed-loop feedback, it is important that the Koopman model remains accurate for reasonably long-time horizons.

### C. Learning Koopman Models: Challenges and Related Work

Learning Koopman representations for nonlinear systems has typically not constrained the properties of the learned model to match those of the original system, such as stability. Instead, most efforts compute Koopman approximations that best evolve states across a single time step. For example, work in [43] makes assumptions on the stability of the underlying nonlinear dynamics (i.e., that it has a single attractor that is (asymptotically) stable), but does not enforce similar constraints on the learned model. As a result, by overlooking the physical properties of the system and not constraining the learning model, stable nonlinear dynamics are sometimes erroneously represented by Koopman operators that are unstable, due to noise, poor quality (e.g. sparse or highly-correlated) measurements, or even limitations of the numerical schemes used [44]–[46]. When the properties of the underlying system and the learned model do not match, the long-term evolution of the states using the Koopman operator increasingly diverges from the true solution.

Few studies have focused on learning Koopman representations with emphasis on long-term accuracy. Work in [47] computes error bounds of Dynamic Mode Decomposition, closely related to the Koopman operator, but the analysis is applicable only to systems with parabolic partial differential equations and has restrictive assumptions on the stability of the identified dynamics. Work in [48] uses deep learning to identify Koopman eigenfunctions from data and considers a loss function that measures the long-term accuracy of the Koopman operator for arbitrary number of steps into the future. However, the final solution is not guaranteed to match the properties of the underlying dynamics and no property of the underlying dynamics is imposed on the learned model.

Further, the optimization complexity grows with the number of prediction steps and, given that deep learning requires large data-sets with rich measurements (diverse parts of the state space), the proposed method scales poorly to high-dimensional systems or long prediction horizons.

There are also only few studies that impose physics-based properties on the Koopman operator. Work in [49] learns Koopman operators under dissipativity constraints and, to the best of our knowledge, is the first study that tries to exploit *a priori* information about the nonlinear dynamics. However, the analysis assumes that the supply rate that describes the dissipativity of the system is known and available for learning, which is not always the case. Further, the authors do not discuss restrictions that dissipative Koopman operator place on the basis functions. For example, inverse functions that diverge at the equilibrium are inconsistent with a dissipative representation and cannot be part of the learned Koopman model. Last, because the optimization problem is numerically intractable, the authors compute solutions to approximate objectives instead.

#### D. Contribution and Structure

This work considers the computation of stable Koopman operators for the purposes of both explicitly minimizing long-term prediction error and learning models that are consistent with the physical properties of the underlying dynamics. Specifically, we

- derive the global (in time) error induced by approximate Koopman models as motivation for generating stable operators,
- use a method to compute (asymptotically) stable Koopman operators,
- provide properties for choosing appropriate basis functions such that the Koopman model is consistent with the stability properties of the underlying nonlinear system, and
- present a method to construct Lyapunov functions for nonlinear dynamics, subject to conditions on the data-driven error.

As the derived global error formula shows, even when the original dynamics are unstable, a stable Koopman operator can outperform the unconstrained (unstable) Koopman approximation. We illustrate, later in Section V, the benefit in performance using as an example the dynamics of a quadrotor, a system that is not inherently stable.

This paper is structured as follows. Section II reviews the Koopman Operator framework for prediction and control of nonlinear systems. Section III i) derives a global error formula for arbitrary Koopman representations, ii) presents necessary conditions for the Koopman representation to be consistent with the stability properties of the underlying nonlinear dynamics, and iii) derives a method for constructing Lyapunov functions for nonlinear systems using stable approximate Koopman operators. Section IV introduces the proposed algorithm to compute stable operators that are nearby solutions to the least-squares error optimization. Section V demonstrates the computation of stable Koopman operators and compares

the prediction and control of nonlinear systems using the unconstrained Koopman operator and the stable Koopman operator. Section VI summarizes the findings and discusses areas that merit further investigation.

## II. KOOPMAN OPERATOR

The Koopman operator  $\mathcal{K} \in \mathbb{R}^{W \times W}$  [22] linearly evolves functions of the states  $s(t) \in \mathcal{S} \subseteq \mathbb{R}^N$  (i.e.  $\Psi(s(t)) \in \mathcal{L} \subseteq \mathbb{R}^W$ , called the observables) without loss of accuracy. Formally, the continuous- and discrete-time operators are respectively given by

$$\frac{d}{dt} \Psi(s(t)) = \mathcal{K} \Psi(s(t)) \quad \text{or} \quad \Psi(s(t_k + \Delta t)) = \mathcal{K}_d \Psi(s(t_k)),$$

where the two operators are linked via  $\mathcal{K} = \log(\mathcal{K}_d)/\Delta t$ . Although a linear representation, the Koopman operator evolves nonlinear dynamics with full fidelity throughout the state space, contrary to methods that locally linearize dynamics around a point or a trajectory.

#### A. Data-Driven Approximations of Koopman Operators

Except for few dynamical structures that admit invariant subspaces [28], Koopman operators are typically infinite-dimensional and make practical use challenging. Even when there is not a finite-dimensional operator that can capture the nonlinear dynamics with full fidelity, there is still interest in obtaining finite-dimensional approximations for the purposes of system identification and control [1], [2], [50]. The finite-dimensional operators are learned as least-squares solutions, typically of the local, one time-step, error across  $P$  measurements. That is

$$\tilde{\mathcal{K}}_d^* = \underset{\tilde{\mathcal{K}}_d}{\operatorname{argmin}} \sum_{k=1}^P \frac{1}{2} \|\Psi(s_k(t_k + \Delta t), u_k(t_k + \Delta t)) - \tilde{\mathcal{K}}_d \Psi(s_k(t_k), u_k(t_k))\|^2. \quad (1)$$

Each measurement  $k$  consists of the initial state  $s_k(t_k)$ , final state  $s_k(t_k + \Delta t)$  and the actuation applied at the same instants,  $u_k(t_k)$  and  $u_k(t_k + \Delta t)$ , respectively. Note that the time spacing  $\Delta t$  between measurements  $s_k(t_k)$  and  $s_k(t_k + \Delta t)$  must be consistent for all  $P$  training measurements. Other regression methods have been used, such as Least Absolute Shrinkage and Selection Operator (LASSO) regression [2], [51], but for simplicity we will use (1) throughout this study without loss of generality. Expression (1) has a closed-form expression

$$\tilde{\mathcal{K}}_d^* = \mathcal{A} \mathcal{G}^\dagger, \quad (2)$$

with

$$\mathcal{A} = \sum_{k=1}^P \Psi(s_k(t_k + \Delta t), u_k(t_k + \Delta t)) \Psi(s_k(t_k), u_k(t_k))^T$$

and

$$\mathcal{G} = \sum_{k=1}^P \Psi(s_k(t_k), u_k(t_k)) \Psi(s_k(t_k), u_k(t_k))^T$$

where  $\dagger$  is the Moore-Penrose pseudoinverse.

### B. Control of Nonlinear Dynamics Using Koopman Operators

Consider a linear system with states  $s(t) \in \mathbb{R}^N$ , control  $u(t) \in \mathbb{R}^M$ , and a discrete-time performance objective

$$J = \sum_{t_k=0}^{\infty} \|s(t_k) - s_{des}(t_k)\|_Q^2 + \|u(t_k)\|_R^2, \quad (3)$$

where  $Q \succeq 0 \in \mathbb{R}^{N \times N}$  and  $R \succ 0 \in \mathbb{R}^{M \times M}$  are weights on the deviation from the desired states and the applied control, respectively. Next, we use the Koopman operator dynamics to design an equivalent objective function and a control response for the original nonlinear system.

To simplify the analysis, we choose basis functions that depend separately on the states and control. That is, we consider basis functions  $\Psi(s(t_k), u(t_k)) = [\Psi_s(s(t_k)), \Psi_u(u(t_k))]^T$ , where  $\Psi_s(s(t_k)) \in \mathbb{R}^{W_s}$  are the Koopman basis functions that depend only on the states, and  $\Psi_u(u(t_k)) \in \mathbb{R}^{W_u}$  indicates those that depend on the input, such that  $W = W_s + W_u$ .

$$\begin{aligned} \Psi(s(t_k + \Delta t), u(t_k + \Delta t)) &= \begin{bmatrix} \Psi_s(s(t_k + \Delta t)) \\ \Psi_u(u(t_k + \Delta t)) \end{bmatrix} \\ &\approx \begin{bmatrix} A & B \\ \cdot & \cdot \end{bmatrix} \begin{bmatrix} \Psi_s(s(t_k)) \\ \Psi_u(u(t_k)) \end{bmatrix}, \end{aligned}$$

where  $(\cdot)$  is used to indicate the terms associated with the evolution of control, which is of no interest here as it will be determined by the feedback policy. The terms  $A \in \mathbb{R}^{W_s \times W_s}$  and  $B \in \mathbb{R}^{W_s \times W_u}$  are sub-matrices of  $\tilde{\mathcal{K}}_d$  and are fixed unless  $\tilde{\mathcal{K}}_d$  is updated. Note that the dynamical equation has been modified to allow for control inputs [23]. The dynamics of the Koopman states are then

$$\Psi_s(s(t_k + \Delta t)) \approx A\Psi_s(s(t_k)) + B\Psi_u(u(t_k)).$$

Given the Koopman representation, the discrete-time performance objective becomes

$$J_{\tilde{\mathcal{K}}} = \sum_{t_k=0}^{\infty} \|\Psi_s(s(t_k)) - \Psi_s(s_{des}(t_k))\|_{Q_{\tilde{\mathcal{K}}}}^2 + \|u(t_k)\|_R^2, \quad (4)$$

where  $Q_{\tilde{\mathcal{K}}} \succeq 0 \in \mathbb{R}^{W_s \times W_s}$  penalizes the deviation from the desired observable functions  $\Psi_s(s_{des}(t_k))$ . We set

$$Q_{\tilde{\mathcal{K}}} = \begin{bmatrix} Q & 0 \\ 0 & 0 \end{bmatrix},$$

where the first  $N$  observables are the original states  $s$  so that a meaningful comparison can be made with regards to the original nonlinear system and the objective in (3).

The Koopman representation is conducive to linear quadratic regulator (LQR) feedback of the form

$$u(t_k) = -K_{LQR}(\Psi_s(s(t_k)) - \Psi_s(s_{des}(t_k))). \quad (5)$$

where  $K_{LQR} \in \mathbb{R}^{M \times N}$  are the LQR gains.

### III. STABLE KOOPMAN OPERATORS

This section derives a formula for the error induced by an approximate Koopman operator for an arbitrary number of time-steps into the future, which motivates the computation of stable Koopman operators, sometimes even in cases when the underlying system is stable. Later in the section, we present

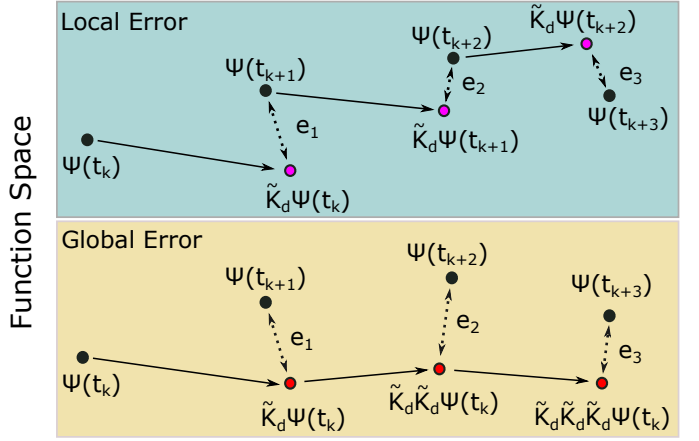


Fig. 1: Local vs Global Koopman error.

an algorithm to compute stable Koopman operators that are nearest, in the Frobenius norm sense, to the unconstrained solutions of the least-squares error optimization (2).

#### A. Global Error of Approximate Koopman Operators: Motivation for Stability

1) *Notation:* In this section only, we use  $t_n \triangleq t_0 + n\Delta t$  to refer to the time propagated  $n \in \mathbb{Z}^+$  steps into the future. This is different than  $t_k$  used throughout the rest of the paper, which indicates the time of  $k$  state measurement. At time  $t_n$ , we use  $\Psi(s(t_n))$  to indicate the true value of the basis function evaluated using the true state value  $s(t_n)$  and  $\tilde{\Psi}_n$  to indicate the approximate solution. We use  $e_n$  to be the local error at the  $n$ th time step induced by the approximate Koopman operator  $\tilde{\mathcal{K}}_d$ , that is

$$e_n \equiv \Psi(s(t_n)) - \tilde{\mathcal{K}}_d\Psi(s(t_{n-1})), \quad (6)$$

which assumes that you always propagate the correct solution  $\Psi(s(t_{n-1}))$  from the previous time step. Similarly, we use  $E_n$  to refer to the global error at time step  $t_n$ :

$$E_n \equiv \Psi(s(t_n)) - \tilde{\mathcal{K}}_d^n\Psi(s(t_0)), \quad (7)$$

which, for  $n = 1$ , matches the local error (6). However, note that the global error (7) is not an accumulation of the local errors (6):  $E_n \neq \sum_i^n e_i$ .

2) *Derivation of Global Error:* Consider the true solution at some time step  $t_n$ , which can be written according to (6) as

$$\Psi(s(t_n)) = \tilde{\mathcal{K}}_d\Psi(s(t_{n-1})) + e_n. \quad (8)$$

Similarly,

$$\Psi(s(t_{n-1})) = \tilde{\mathcal{K}}_d\Psi(s(t_{n-2})) + e_{n-1}. \quad (9)$$

Plugging (9) into (8)

$$\begin{aligned} \Psi(s(t_n)) &= \tilde{\mathcal{K}}_d(\tilde{\mathcal{K}}_d\Psi(s(t_{n-2})) + e_{n-1}) + e_n \\ &= \tilde{\mathcal{K}}_d^2\Psi(s(t_{n-2})) + \tilde{\mathcal{K}}_d e_{n-1} + e_n. \end{aligned}$$

Recursively expressing the solution in terms of the previous solution and the corresponding local error yields

$$\Psi(s(t_n)) = \tilde{\mathcal{K}}_d^n \Psi(s(t_0)) + \sum_{i=0}^{n-1} \tilde{\mathcal{K}}_d^i e_{n-i},$$

where

$$\tilde{\Psi}_n = \tilde{\mathcal{K}}_d^n \Psi(s(t_0))$$

is the Koopman estimate at time step  $t_n$ . Therefore, the global error at  $t_n$ , defined in (7), is

$$E_n = \sum_{i=0}^{n-1} \tilde{\mathcal{K}}_d^i e_{n-i},$$

which can be easily shown to simplify back to (7).

3) *Global Error Bound*: For invariant subspaces, there is no local or global error, that is

$$\|e_{max}\| = 0 \iff \|E_{k+n}\| = 0.$$

Next, we try to compute a bound for the global (in time) error bound.

$$\begin{aligned} \|E_n\| &= \left\| \sum_{i=0}^{n-1} \tilde{\mathcal{K}}_d^i e_{n-i} \right\| \\ &\leq \sum_{i=0}^{n-1} \|\tilde{\mathcal{K}}_d^i e_{n-i}\| \\ &\leq \sum_{i=0}^{n-1} \|\tilde{\mathcal{K}}_d^i\| \cdot \|e_{n-i}\|. \end{aligned}$$

Using the property  $\|AB\| \leq \|A\| \cdot \|B\|$ ,

$$\|E_n\| \leq \sum_{i=0}^{n-1} \|\tilde{\mathcal{K}}_d\|^i \cdot \|e_{n-i}\|.$$

Assuming that the local error is bounded, meaning there exists  $\|e_{max}\|$  such that  $\|e_i\| \leq \|e_{max}\| \forall i \in [1, n]$ , then, we can simplify the above expression to

$$\|E_n\| \leq \|e_{max}\| \cdot \sum_{i=0}^{n-1} \|\tilde{\mathcal{K}}_d\|^i. \quad (10)$$

For invariant subspaces, there is no local or global error, that is

$$\|e_{max}\| = 0 \iff \|E_{k+n}\| = 0.$$

Note that the power of the matrix norm diverges as the number of prediction time steps increases unless  $\tilde{\mathcal{K}}_d$  is stable, which, for the discrete-time case, means that i) all of its eigenvalues lie within the unit circle of the complex plane or ii) all eigenvalues lie inside or on the unit circle and the eigenvalues that lie on the unit circle have equal algebraic and geometric multiplicity [52]–[56].<sup>1</sup>

Therefore, an unstable operator  $\tilde{\mathcal{K}}_d$  amplifies even small errors rendering the long-term prediction of the Koopman representation inaccurate. Instead, we propose that one should

<sup>1</sup>Algebraic multiplicity of  $\lambda_i$  is the number of roots of  $\det(\lambda I - A)$ ; geometric multiplicity of  $\lambda_i$  is the number of linearly independent eigenvectors  $v_i$  for  $Av_i = \lambda_i v_i$ .

use, if there exists, a nearby stable operator that generates comparatively similar local errors.

In the absence of invariant subspaces, no finite-dimensional operator can propagate the dynamics without error. If the original dynamics are globally unstable, the system states diverge and there does not exist a bounded local error  $\|e_{max}\|$ ; then, the global error, whether using a stable or unstable Koopman operator, grows unbounded. If the original dynamics are globally stable, then the global error is bounded only if the identified operator  $\tilde{\mathcal{K}}_d$  is stable. Even if dynamics are not globally stable, but provided that the system states are bounded and do not diverge such that there exists a bounded local error  $\|e_{max}\|$ , then the global error is bounded using a stable Koopman operator and diverges otherwise.

As pointed out in [57], the eigenvalue profile of  $\tilde{\mathcal{K}}_d$  can be misleading in terms of bounding the power of the operator, because the upper bound can be itself large. Although we take note, such scenarios are shown to occur for moderately large dimensions of the operator ( $W \approx 100$ ) and do not apply in the examples of this paper. Exploiting the conditions that prevent large error growth in the transient response of a system, which is related to the strong stability property [58], for high-dimensional operators is left for future work [57], [59], [60].

Next, we discuss necessary conditions for the Koopman basis functions such that they are consistent with the dynamics of a stable (or an asymptotically stable) operator. We further relate the stability properties of the Koopman representation to the stability properties of the original nonlinear dynamics. The analysis is performed in the continuous-time where system dynamics are typically expressed in.

### B. Stability-Based Conditions for Koopman Basis Functions

Consider a nonlinear dynamical system with states  $s(t) \in \mathbb{R}^N$  and dynamics of the form

$$\frac{d}{dt} s(t) = f(s(t)). \quad (11)$$

and the associated Koopman representation of the nonlinear dynamical system (11)

$$\frac{d}{dt} \Psi(s(t)) = \mathcal{K} \Psi(s(t)). \quad (12)$$

If  $\lambda_1, \dots, \lambda_W$  are the eigenvalues of the Koopman operator, then the system is stable if the Koopman operator is stable, that is  $\text{Re}[\lambda_i] \leq 0$  for all  $i = 1, \dots, W$ , and the eigenvalues with zero real part have equal algebraic and geometric multiplicity [52]. Similarly, the system is asymptotically stable if the Koopman operator is Hurwitz, that is  $\text{Re}[\lambda_i] < 0$  for all  $i = 1, \dots, W$ . Similar eigenvalue conditions exist for discrete-time operators.

If the two representations (11) and (12) are equivalent throughout the state space without loss of accuracy, then we present certain properties that we assume must be true.

**Assumption 1.** *For a nonlinear dynamical system (11) and its equivalent Koopman representation (12), the following must be true:*

1) A trajectory  $s^*(t)$  is an equilibrium for the nonlinear dynamical system (11) if and only if it is an equilibrium for the Koopman dynamics (12). That is,

$$f(s^*(t)) = 0 \iff f(\Psi(s^*(t))) = 0.$$

2) A trajectory  $s^*(t)$  is Lyapunov stable for the nonlinear dynamical system (11) if and only if it is Lyapunov stable for the Koopman dynamics (12). That is,

$$\|s(t)\| < \epsilon_s \iff \|\Psi_i(s(t))\| < \epsilon_\Psi \quad \forall i \in \mathbb{Z}^{+2}, \quad t \geq 0,$$

where  $\epsilon_s > 0$  and  $\epsilon_\Psi > 0$ .

3) A trajectory  $s^*(t)$  is asymptotically stable in  $\mathcal{D} \subseteq \mathbb{R}^N$  for the nonlinear dynamical system (11) if and only if it is asymptotically stable in  $\mathcal{D} \subseteq \mathbb{R}^N$  for the Koopman dynamics (12). That is, given  $s(0) \in \mathcal{D}$ ,

$$\lim_{t \rightarrow \infty} s(t) = 0 \iff \lim_{t \rightarrow \infty} \Psi(s(t)) = 0.$$

Note that the conditions on the Koopman basis functions in Assumption 1 consider Koopman representations that are equivalent to the nonlinear dynamics. Even when that is not the case and only an approximate Koopman operator is available, these assumptions must still hold in order for the learned model to be consistent with the stability properties of the original nonlinear dynamics.

In the following subsections, we present, in the form of Theorems, necessary conditions for the stability properties of Koopman operators. These conditions must be met even for approximate Koopman operators in order to match the stability properties of the original system. We use the Theorems to motivate placing appropriate stability properties on the learned Koopman representations.

1) *Conditions on Koopman Operators for Stable Systems:*

In this subsection, we investigate the conditions placed on a Koopman representation that shares all the stability properties of an underlying stable, in the sense of Lyapunov, system. The analysis rests on the following assumption.

**Assumption 2.** All states  $s(t) \in \mathbb{R}^N$  of a nonlinear dynamical system (11) remain bounded for all  $t$ . That is, for some  $\epsilon \geq 0$ ,  $\|s(t)\| \leq \epsilon$  for all  $t \geq 0$ .

Next, we prove that only a stable Koopman operator can accurately represent nonlinear dynamics that are Lyapunov stable.

**Definition 1.** Given a nonlinear dynamical system (11) with bounded states  $s(t) \in \mathbb{R}^N$ ,  $\mathcal{D}_\epsilon \subseteq \mathbb{R}^N$  denotes the state-space that bounds all states. That is, if  $\|s(t)\| \leq \epsilon$ , then  $s(t) \in \mathcal{D}_\epsilon$  for all  $t \geq 0$ .

**Theorem 1** (Lyapunov Stability—Continuous-time). Consider a nonlinear dynamical system (11) and an equivalent Koopman representation (12). The solution  $s(t) = 0$  is a Lyapunov stable equilibrium if and only if the Koopman operator  $\mathcal{K}$  is stable.

<sup>2</sup>We only constraint the norms of each individual basis function, instead of the norm of  $\Psi$ , to be bounded due to the fact that, for an infinite-dimensional Koopman operator, the sum of norms of basis functions that are individually bounded would still be infinite.

*Proof:* From Assumption 1, if  $s(t) = 0$  is a Lyapunov stable solution for the nonlinear dynamical, then it is also a Lyapunov stable solution for the Koopman dynamics (12). That is,

$$\|s(t)\| < \epsilon_s \implies \|\Psi(s(t))\| < \epsilon_\Psi, \quad t \geq 0.$$

If  $\Psi(s(t)) = 0$  is a Lyapunov stable solution for the Koopman dynamics (12), then  $\mathcal{K}$  is stable.

Further, if  $\mathcal{K}$  is stable, then the  $\Psi(s(t)) = 0$  is a Lyapunov stable equilibrium. Then, from Assumption 1,  $s(t) = 0$  is also a Lyapunov stable equilibrium for the nonlinear dynamical system (11). That is,

$$\|\Psi(s(t))\| < \epsilon_\Psi \implies \|s(t)\| < \epsilon_s, \quad t \geq 0. \quad \blacksquare$$

Theorem 1 proves that a Koopman operator that accurately represents a Lyapunov stable nonlinear system must be stable. Therefore, even approximate Koopman operators must satisfy this condition in order to correctly capture the stability properties. Given a part of the state-space  $\mathcal{D}_\epsilon$  that bounds all trajectories  $s(t)$  of the nonlinear system that start within  $\mathcal{D}_\epsilon$ , a Koopman operator trained with measurements from  $\mathcal{D}_\epsilon$  should be stable (see Theorem 1). Even when no finite-dimensional Koopman representation can capture the nonlinear dynamics with full fidelity, the approximate operator should be stable such that the system states do not grow unbounded and exit  $\mathcal{D}_\epsilon$ . Therefore, it is a necessary and sufficient condition that all eigenvalues of the Koopman operator must be in the left half-plane. In discrete time, the equivalent condition is that all eigenvalues of the discrete-time operator must lie inside the unit circle.

Note that the notion of global stability is considered only in the sense of asymptotic stability and not Lyapunov stability. The system states, even when unbounded, always lie inside  $\mathbb{R}^N$ . Considering the entire (infinite) state space as a region of stability, that is  $\mathcal{D}_\epsilon = \mathbb{R}^N$ , all nonlinear dynamical systems can be thought of as globally Lyapunov stable, a property that carries no meaning.

2) *Conditions on Koopman Operators for Asymptotically Stable Systems:* In this subsection, we investigate the conditions placed on a Koopman representation that shares all the stability properties of an underlying asymptotically stable system. The analysis assumes that all states of a nonlinear dynamical system (11) lie inside a domain of attraction  $D_0 \subseteq \mathbb{R}^N$ , formally defined in Definition 2.

**Definition 2.** Given a nonlinear dynamical system (11) and an asymptotically stable solution  $s(t) = 0$ , the domain of attraction is

$$D_0 \triangleq \{s_0 \in \mathcal{D} : \text{if } s(0) = s_0, \text{ then } \lim_{t \rightarrow \infty} s(t) = 0\}.$$

Further, the analysis rests on the following assumption.

**Assumption 3.** The nonlinear dynamical system (11) has a single asymptotic equilibrium.

Note that for multiple asymptotic equilibria, there need to be separate regions of attractions, which must in turn be represented by separate Koopman operators. In this work, we

focus on obtaining a single Koopman operator consistent with a single asymptotic equilibrium. For many systems, due to the presence of friction, this can often be represented as the zero-velocity state. For nonlinear systems with multiple equilibria points, one can use work in [61] to obtain multiple local Koopman representations.

Next, we prove that only a Hurwitz Koopman operator can accurately represent nonlinear dynamics that are asymptotically stable.

**Theorem 2** (Asymptotic Stability—Continuous-time). *Consider a nonlinear dynamical system (11) and an equivalent Koopman representation (12). The solution  $s(t) = 0$  is an asymptotically stable equilibrium if and only if the Koopman operator  $\mathcal{K}$  is Hurwitz.*

*Proof:* From Assumption 1, if  $s(t) = 0$  is an asymptotically stable solution for the nonlinear dynamical, then it is also an asymptotically stable solution for the Koopman dynamics (12). That is,

$$\lim_{t \rightarrow \infty} s(t) = 0 \iff \lim_{t \rightarrow \infty} \Psi(s(t)) = 0.$$

If  $\Psi(s(t)) = 0$  is an asymptotically stable solution for the Koopman dynamics (12), then  $\mathcal{K}$  must be Hurwitz. That is,

$$\lim_{t \rightarrow \infty} \Psi(s(t)) = 0 \implies \text{Re}[\lambda_i] < 0,$$

for each eigenvalue  $\lambda_i$  of the operator  $\mathcal{K}$ . Similarly, if  $\mathcal{K}$  is Hurwitz, then using the linear dynamics (12),  $\Psi(s(t)) = 0$  is an asymptotically stable equilibrium. That is,

$$\text{Re}[\lambda_i] < 0 \implies \lim_{t \rightarrow \infty} \Psi(s(t)) = 0.$$

Then,

$$\lim_{t \rightarrow \infty} s(t) = 0 \iff \text{Re}[\lambda_i] < 0$$

■

Theorem 2 proves that a Koopman operator that accurately represents an asymptotically stable nonlinear system must be Hurwitz. Therefore, it is a necessary and sufficient condition that all eigenvalues of the Koopman operator must be in the left half-plane. In discrete time, the equivalent condition is that all eigenvalues of the discrete-time operator must lie inside the unit circle.

### C. Lyapunov Functions for Nonlinear Systems Using Koopman Operators

Given a stable operator, it is possible to design Lyapunov functions for nonlinear systems using the data-driven Koopman matrix. Consider a finite-dimensional Koopman representation for general dynamical systems (11) that satisfies Assumption 1 such that

$$\frac{d}{dt} \Psi(s(t)) = \tilde{\mathcal{K}} \Psi(s(t)) + \epsilon(\Psi(s(t))), \quad (13)$$

where

$$\epsilon(\Psi(s(t))) \triangleq f(\Psi(s(t))) - \tilde{\mathcal{K}} \Psi(s(t)) \quad (14)$$

is the residual error.

Such a Koopman operator can be used to design Lyapunov functions for the nonlinear dynamics. Note that the following theorem is relevant to approximate Koopman representations of nonlinear systems, whereas Theorems 1 and 2 consider an accurate Koopman embedding.

**Theorem 3.** *Consider a Koopman representation (13) of a nonlinear dynamical system. Further assume  $\tilde{\mathcal{K}}$  is stable. Let*

$$\alpha \leq \lambda_{\min}(Q) - 2\lambda_{\max}(P),$$

where  $Q \succ 0$  and  $P \succ 0$  is the solution to the Lyapunov equation. If

$\|\epsilon(\Psi(0))\|_2 = 0$  and  $\|\epsilon(\Psi(s(t)))\|_2 < \alpha \|\Psi(s(t))\|_2 \forall t$ , then, the zero solution  $\Psi(s(t)) = 0$  to the nonlinear dynamics is asymptotically stable. Further,  $V = \Psi(s(t))^T P \Psi(s(t))$  is a Lyapunov function.

*Proof:* Consider a candidate Lyapunov function  $V = \Psi^T(s(t)) P \Psi(s(t))$ . Taking the time derivative,

$$\begin{aligned} \frac{d}{dt} V(\Psi(s(t))) &= \frac{dV(\Psi(s(t)))}{d\Psi(s(t))} \frac{d\Psi(s(t))}{dt} \\ &= \Psi(s(t))^T P f(\Psi(s(t))) \\ &\quad + f(\Psi(s(t)))^T P \Psi(s(t)) \\ &= \Psi(s(t))^T P [\mathcal{K} \Psi(s(t)) + \epsilon(\Psi(s(t)))] \\ &\quad + [\Psi^T \tilde{\mathcal{K}}^T + \epsilon(\Psi(s(t)))^T] P \Psi(s(t)) \\ &= \Psi(s(t))^T (P \tilde{\mathcal{K}} + \tilde{\mathcal{K}}^T P) \Psi(s(t)) \\ &\quad + 2\Psi(s(t))^T P \epsilon(\Psi(s(t))). \end{aligned}$$

Given that  $\tilde{\mathcal{K}}$  is stable and  $Q \succ 0$ , then there always exists a (unique) solution  $P \succ 0$  to the Lyapunov equation. Thus,

$$P \tilde{\mathcal{K}} + \tilde{\mathcal{K}}^T P = -Q$$

such that

$$\frac{d}{dt} V(\Psi(s(t))) = -\Psi(s(t))^T Q \Psi(s(t)) + 2\Psi(s(t))^T P \epsilon(\Psi(s(t))).$$

Note that  $-\Psi(s(t))^T Q \Psi(s(t)) \leq -\lambda_{\min}(Q) \|\Psi(s(t))\|_2^2$  and using the Cauchy-Schwartz inequality, it follows that

$$\begin{aligned} \frac{d}{dt} V(\Psi(s(t))) &\leq -\lambda_{\min}(Q) \|\Psi(s(t))\|_2^2 \\ &\quad + 2\lambda_{\max}(P) \|\Psi(s(t))\|_2 \|\epsilon(\Psi(s(t)))\|_2. \end{aligned}$$

Then, using

$$\|\epsilon(\Psi(s(t)))\|_2 < \alpha \|\Psi(s(t))\|_2$$

it follows that

$$\frac{d}{dt} V(\Psi(s(t))) \leq -(\lambda_{\min}(Q) - 2\alpha \lambda_{\max}(P)) \|\Psi(s(t))\|_2^2. \quad (15)$$

Choosing  $\alpha \leq \lambda_{\min}(Q)/2\lambda_{\max}(P)$ , it follows that  $\frac{d}{dt} V(s(t)) \leq 0$  such that the system (13) is stable about  $\Psi(s(t)) = 0$ . Further, if  $\alpha < \lambda_{\min}(Q)/2\lambda_{\max}(P)$ , it follows that  $\frac{d}{dt} V(s(t)) < 0$  and the system is asymptotically stable about  $\Psi(s(t)) = 0$ . ■

In the next Section, we propose a novel way of computing stable Koopman operators that are nearby solutions to the least-squares optimization (1) typically considered in the literature.

#### IV. SYNTHESIS OF STABLE KOOPMAN OPERATORS

This section presents an algorithm for the Data-driven Identification of Stable Koopman Operators (DISKO). The algorithm is inspired by work in [56] that considers the problem of computing the nearest, in the Frobenius norm sense, stable matrix to an unstable one.

Specifically, the authors in [56] consider the minimization problem of

$$\inf_{X \in S_d^{n,n}} \|A - X\|_F^2, \quad (16)$$

where  $A \in \mathbb{R}^{n \times n}$ ,  $X \in \mathbb{R}^{n \times n}$ , and use a gradient descent algorithm to compute a local minimum solution that is guaranteed to be stable. They are able to do so by proving that a matrix  $A$  is stable if and only if it can be written as  $A = S^{-1}UBS$ , where  $S$  is positive definite,  $U$  is orthogonal, and  $B$  is a positive semidefinite contraction; its singular values are less than or equal to 1. Using the Koopman notation, stabilizing the operator would take the form

$$\inf_{\tilde{\mathcal{K}}_d \in S_d^{n,n}} \|\tilde{\mathcal{K}}_d^* - \tilde{\mathcal{K}}_d\|_F^2. \quad (17)$$

##### A. Stable Least-Squares Koopman Operators

In this work, we are interested in computing a stable matrix that is the nearest solution to the least squares error, not simply the nearest, in the Frobenius norm sense, stable matrix as in (17). To be able to compute a stable Koopman operator, we first convert the optimization (18) to an equivalent formulation.

**Proposition 1.** Consider  $P$  measurements of states  $s \in \mathbb{R}^N$  and basis functions  $\Psi(s(t)) \in \mathbb{R}^W$ . Given  $X$  and  $Y$  such that

$$X = \begin{bmatrix} \Psi(s_1(t_1), u_1(t_1))^T \\ \vdots \\ \Psi(s_P(t_P), u_P(t_P))^T \end{bmatrix}^T$$

and

$$Y = \begin{bmatrix} \Psi(s_1(t_1 + \Delta t), u_1(t_1 + \Delta t))^T \\ \vdots \\ \Psi(s_P(t_P + \Delta t), u_P(t_P + \Delta t))^T \end{bmatrix}^T.$$

expression

$$\sum_{k=1}^{P-1} \frac{1}{2} \|\Psi(s_{k+1}, u_{k+1}) - \tilde{\mathcal{K}}_d \Psi(s_k, u_k)\|_F^2$$

is equivalent to

$$\|Y - \tilde{\mathcal{K}}_d X\|_F^2,$$

where  $X, Y \in \mathbb{R}^{N \times P}$ ,  $\tilde{\mathcal{K}}_d \in \mathbb{R}^{N \times N}$ ,  $\|\cdot\|_F$  is the Frobenius norm of a matrix and  $S_d^{n,n}$  is the set of all stable matrices of size  $N \times N$ .

*Proof:* See Appendix A. ■

From Proposition 1, seeking stable Koopman operators for

$$\inf_{\tilde{\mathcal{K}}_d \in S_d^{n,n}} \|Y - \tilde{\mathcal{K}}_d X\|_F^2, \quad (18)$$

is equivalent to seeking stable solutions for (1).

Note that solving (18) is not equivalent to projecting the unconstrained Koopman solution (1) to the stable set of matrices. That is,

$$\inf_{\tilde{\mathcal{K}}_d \in S_d^{n,n}} \|Y - \tilde{\mathcal{K}}_d X\|_F^2 \neq \inf_{\tilde{\mathcal{K}}_d \in S_d^{n,n}} \|\tilde{\mathcal{K}}_d^* - \tilde{\mathcal{K}}_d\|_F^2. \quad (19)$$

Projecting an unstable solution of (1) to the stable set results in a matrix that is stable but often with much greater fitness error than the solution to (18), as we demonstrate with examples later in this Section.

Using the property that a matrix  $A$  is stable if and only if it can be written as  $A = S^{-1}UBS$  [56], we reformulate the optimization (18) such that

$$\inf_{K_d \in S_d^{n,n}} \|Y - K_d X\|_F^2 = \inf_{S > 0, U \text{ orthogonal}, B \succeq 0, \|B\| \leq 1} \|Y - S^{-1}UBS X\|_F^2 \quad (20)$$

and use a gradient-descent algorithm (recently submitted as separate work) to find locally optimal stable solutions  $\tilde{\mathcal{K}}_d$ . Let  $f(S, U, B) = \|Y - S^{-1}UBS X\|_F^2$ . The gradients with respect to  $S$ ,  $U$ , and  $B$  are given by

$$\begin{aligned} \nabla_S f(S, U, B) &= -S^{-T}(S^{-1}UBS X - Y)X^T S^T B^T U^T S^{-T} \\ &\quad + B^T U^T S^{-T}(S^{-1}UBS X - Y)X^T \\ \nabla_U f(S, U, B) &= -S^{-T}(Y - S^{-1}UBS X)X^T S^T B^T \\ \nabla_B f(S, U, B) &= -U^T S^{-T}(Y - S^{-1}UBS X)X^T S^T \end{aligned} \quad (21)$$

which, for  $\mathcal{Z} = S^{-1}UBS$  and  $\mathcal{V} = (\mathcal{Z}X - Y)X^T$ , simplifies to

$$\begin{aligned} \nabla_S f(S, U, B) &= -S^{-T}[\mathcal{V}\mathcal{Z}^T + \mathcal{Z}^T\mathcal{V}] \\ \nabla_U f(S, U, B) &= S^{-T}\mathcal{V}S^T B^T \\ \nabla_B f(S, U, B) &= U^T S^{-T}\mathcal{V}S^T. \end{aligned}$$

The derivation of the gradients will be soon available in a recently submitted paper.

The gradient descents (21) depend on  $X$  and  $Y$ , which contain a history of all the basis functions measurements and can slow down the computation over time, as increasingly more data are collected. To speed up the computation, we use the relationship  $XX^T = \mathcal{G}$  and  $YX^T = \mathcal{A}$  (derived in Appendix B) such that  $\mathcal{V} = \mathcal{Z}\mathcal{G} - \mathcal{A}$  can be incrementally updated with new measurements and preserve memory space.

## V. RESULTS

### A. Least-Squares vs Nearest Stabilization

In this section, we demonstrate the performance of the proposed DISKO algorithm that solves the least squares stabilization problem (18). We compare Koopman solutions to the direct stabilization method (17) that does not consider the least-squares fitness error and also compare the evolution of nonlinear dynamics using the approximate Koopman operator solutions from (1) and (18).

**Algorithm 1:** DISKO

---

**Data:**  $X, Y \in \mathbb{R}^{W \times P}$   
**Result:** Stable  $\tilde{\mathcal{K}}_d \in \mathbb{R}^{W \times W}$

1 Initialize  $\tilde{\mathcal{K}}_d$ ,  $\gamma$ , fast gradient descent parameter  $\alpha_1$ ;  
2 **while**  $k < k_{max}$  **do**  
3    $e = \|Y - \tilde{\mathcal{K}}_d X\|_F^2$ ;  
4    $e_{temp} = \infty$ ;  
5   **while**  $e_{temp} > e$  **and**  $\gamma \geq \gamma_{min}$  **do**  
6      $S_k = S - \gamma \nabla_S f(S, U, B)$ ;  
7      $U_k = U - \gamma \nabla_U f(S, U, B)$ ;  
8      $B_k = B - \gamma \nabla_B f(S, U, B)$ ;  
9      $\tilde{\mathcal{K}}_d = S^{-1} U B S$  ;  
10      $\gamma = \frac{2}{3} \gamma$ ;  
11      $e_{temp} = \|Y - \tilde{\mathcal{K}}_d X\|_F^2$ ;  
12   **end**  
13   **if**  $\gamma < \gamma_{min}$  **then**  
14     Restart fast gradient descent  
15   **else**  
16      $\alpha_{k+1} = \frac{1}{2} (\sqrt{\alpha_k^4 + 4\alpha_k^2} - \alpha_k^2)$ ;  
17      $\beta_{k+1} = \frac{\alpha_k(1-\alpha_k)}{\alpha_k^2 + \alpha_{k+1}}$ ;  
18      $S = S_k$ ;  
19      $U = U_k$ ;  
20      $B = B_k$ ;  
21      $\tilde{\mathcal{K}}_d = S^{-1} U B S$   
22   **end**  
23 **end**


---

*Randomly Unstable Input:* Consider the randomly generated matrices

$$X = \begin{bmatrix} 0.1419 & 0.4218 & 0.9157 & 0.7922 & 0.9595 \\ 0.6557 & 0.0357 & 0.8491 & 0.9340 & 0.6787 \\ 0.7577 & 0.7431 & 0.3922 & 0.6555 & 0.1712 \end{bmatrix}$$

$$Y = \begin{bmatrix} 8.1472 & 9.0579 & 1.2699 & 9.1338 & 6.3236 \\ 0.9754 & 2.7850 & 5.4688 & 9.5751 & 9.6489 \\ 1.5761 & 9.7059 & 9.5717 & 4.8538 & 8.0028 \end{bmatrix}.$$

Computing the least-squares solution using (1) and then projecting it to the stable set of matrices using (17) yields

$$\tilde{\mathcal{K}}_d = \begin{bmatrix} 0.0041 & -6.6031 & 5.1709 \\ 10.3449 & -1.9480 & -0.0590 \\ 11.7192 & -6.7149 & 3.4609 \end{bmatrix},$$

with eigenvalues  $\Lambda = \{0.87, 0.87, -0.22\}$ . The least-squares error using the stable matrix is

$$\|Y - \tilde{\mathcal{K}}_d X\|_F^2 = 406.07$$

and the Frobenius norm from the least squares solution is

$$\|\tilde{\mathcal{K}}_d^* - \tilde{\mathcal{K}}_d\|_F^2 = 91.95.$$

On the other hand, directly solving (18) generates a very different solution

$$\tilde{\mathcal{K}}_d = \begin{bmatrix} 5.6337 & -8.2334 & 11.5883 \\ 14.4877 & -5.0863 & 1.9636 \\ 8.3346 & -2.8916 & 1.0662 \end{bmatrix}$$

with eigenvalues  $\Lambda = \{0.98, 0.98, -0.35\}$ . The least-squares error using the stable matrix is

$$\|Y - \tilde{\mathcal{K}}_d X\|_F^2 = 158.94$$

and the Frobenius norm from the least squares solution is

$$\|\tilde{\mathcal{K}}_d^* - \tilde{\mathcal{K}}_d\|_F^2 = 217.06.$$

As expected, projecting the unstable solution to the stable set and ignoring the least-squares error fitness generates a solution that is closer, in the Frobenius norm sense, to the original unstable matrix, but also with greater error compared to the solution of (18). This is why the Algorithm in [56] is not suitable for solving (18).

### B. Comparisons of Reconstruction and Prediction Error

We compare the proposed DISKO algorithm to the algorithm in [62], which is shown to outperform the rest state-of-the-art algorithms. The algorithms are compared on finding stable operators that minimize the error in (18) for varying number of basis functions ( $W \in [2, 100]$ ) and number of measurements ( $P \in [2, 100]$ ). Data in  $X$  are sampled from a uniform distribution  $U(0, 10)$  and data in  $Y$  are sampled from a uniform distribution  $U(0, 20)$ , where  $U(a, b)$  is a uniform distribution where  $a$  and  $b$  are the minimum and maximum values, respectively. The results are presented in Fig. 2. DISKO outperforms CG in all cases, for any number of measurements and functions used. Further, CG does not always converge to a solution.

Next, we compare the evolution of the nonlinear dynamics of a pendulum using the solutions of (1) and (18). The way (18) modifies the eigenvalues subject to the least-squares minimization is shown in Fig. 3 and the long-term accuracy of the two solutions is shown in Fig. 4. While the evolution under the Koopman operator from (1) diverges away, the states remain bounded under the stable operator obtained with (18). Using a Monte Carlo sampling on initial conditions, we compare the prediction error on the pendulum angle as a function of the number of training measurements, shown in Fig. 5a. The stable Koopman operator leads to smaller average prediction error for any number of measurements used for training, as well as lower error spread than the least-squares, unconstrained solution (1). Note that the envelope of the standard deviation error of the unconstrained Koopman is slightly lower than the stable solution around 10 training measurements, suggesting that it is possible that the stable Koopman gives at times a larger error. However, that is a result of the unstable Koopman overfitting to certain initial conditions and accurately predicting the evolution of very few initial states. Also note that there is a large error spike for the unstable Koopman model around 5 measurements, which demonstrates that the unstable solution can be very inaccurate when trained with few measurements; on the other hand, the error for the stable Koopman operator does not have large error spikes no matter how few measurements are used.

When few measurements are available, the least squares solution is prone to misidentifying the system. To emphasize the benefit of stable operators in the low-sample limit, we next

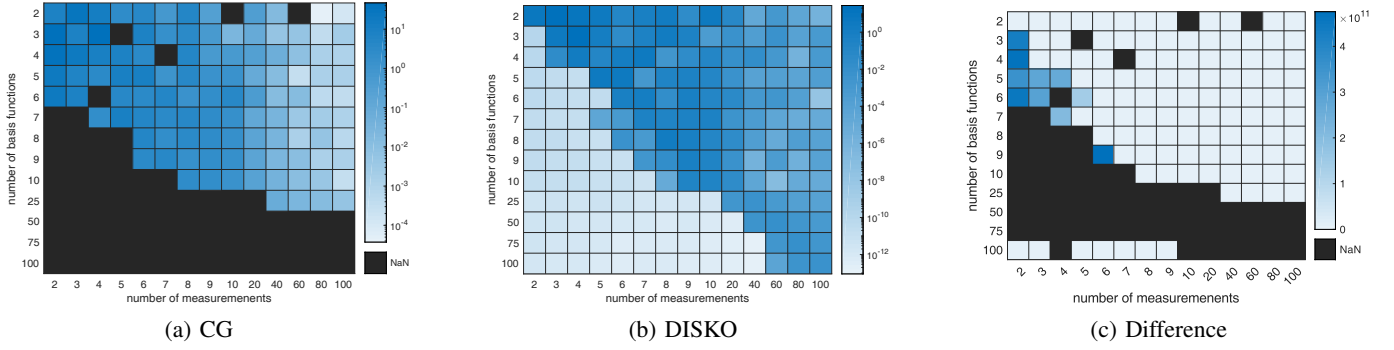


Fig. 2: Comparison of DISKO and CG [62] for random data of varying number of measurements and numbers of basis functions. The error is normalized by the product of the number of measurements and functions. In 2c, the difference is the percent difference of the error between the two algorithms and is calculated as  $\frac{e_{CG} - e_{DISKO}}{e_{DISKO}}$ .

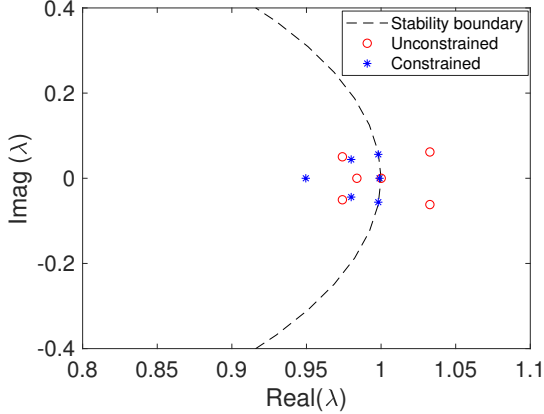


Fig. 3: Eigenvalues of the unconstrained (1) and constrained (18) Koopman operator for the nonlinear dynamics of a pendulum. The constrained operator pushes the unstable eigenvalues to the stability boundary. The stable eigenvalues are also appropriately modified so that constrained Koopman solution locally minimizes the prediction error (18).

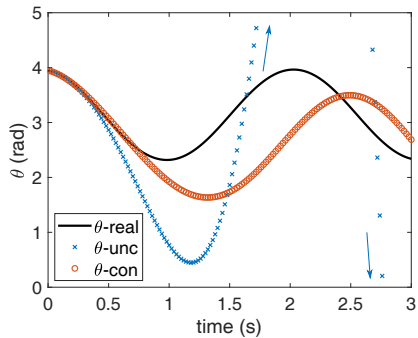


Fig. 4: Prediction of the angle of the pendulum system using the unconstrained Koopman solution (1) and the constrained-stable Koopman operator. The predictions of the unconstrained Koopman operator start to diverge away from the pendulum states after 1 second.

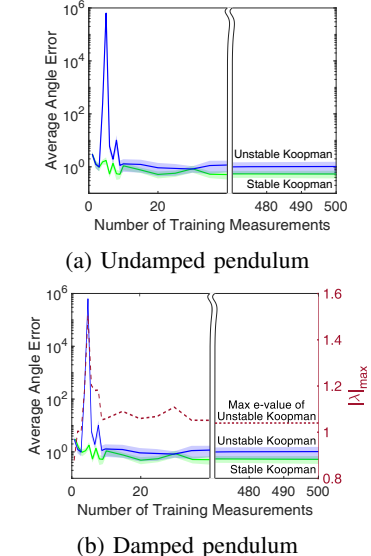


Fig. 5: Average angle error, with one-half standard deviation shading, for the undamped (Fig. 5a) and damped (Fig. 5b) pendulum dynamics, as predicted by the unconstrained and the constrained-stable Koopman operator solutions. For each number of measurements used to compute a Koopman operator, the average angle error is the average absolute difference of the true system state (evolved using the nonlinear dynamics) and the system state as predicted by either Koopman operator over 1 second over 300 initial conditions.

compare the average angle error when the training samples are few. The results, using the dynamics of a damped pendulum, are shown in Fig. 5b. The error spike around 10 measurements is a result of the expected overfitting when few measurements are available. The constrained Koopman on the other hand maintains a similar error profile independent of the number of training samples. Note again that the average error is lower for the stable Koopman operator for all number of training measurements.

Next, we use a stable Koopman operator to predict the unknown dynamics of a hopper system. The results are shown in Fig. 6.

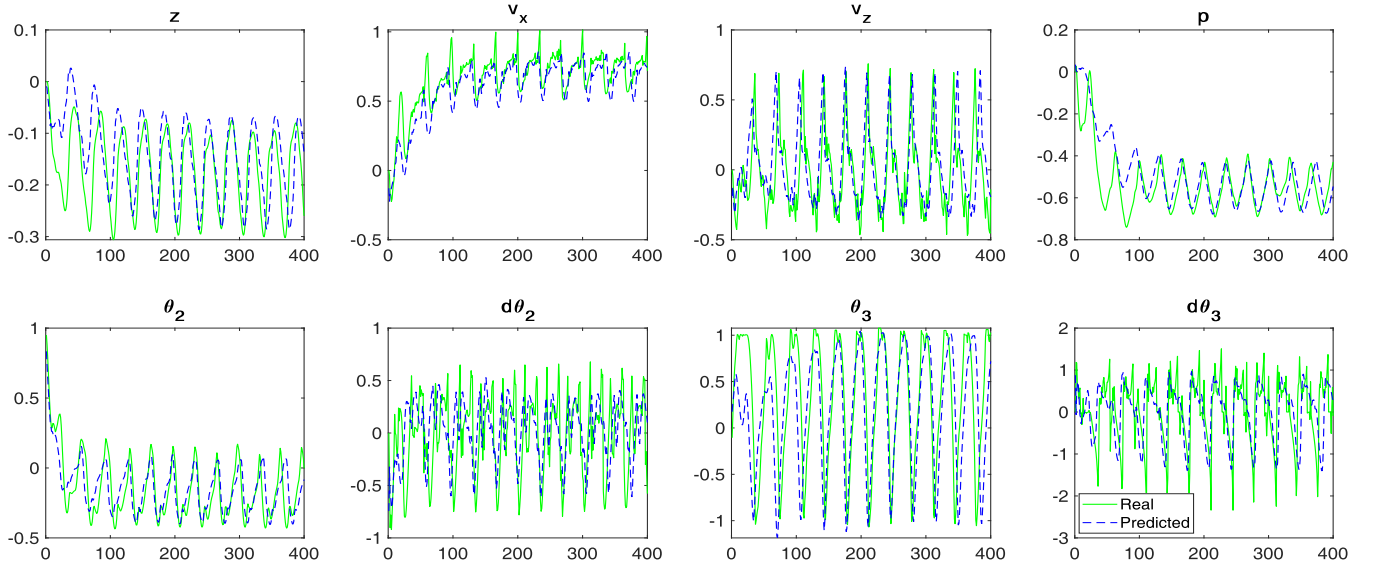


Fig. 6: Prediction of hopper states with stable Koopman Operator over 400 time steps.

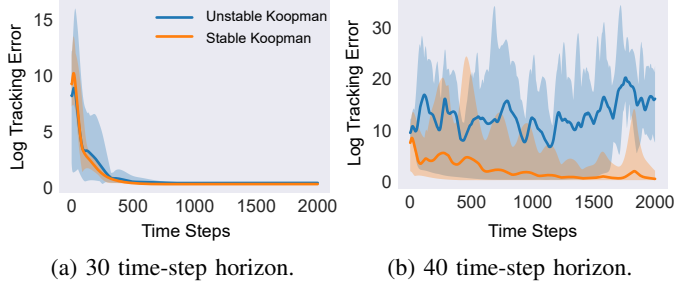


Fig. 7: Log error of the tracking cost using the dynamics of a quadrotor. The performance of an LQR policy derived from the stable (18) and unstable (1) Koopman operators is compared. Both models collect measurements with active learning. At the end of the learning phase, the stable Koopman is computed and the LQR gains from both models are derived. The solid line represents the median score of each approach and the shaded envelope the lowest and highest cost.

### C. Nonlinear Control Using Stable Koopman Operators

In this section, we demonstrate the benefit of using stable Koopman operators for nonlinear control. Using the dynamics of a quadrotor, we collect measurements using active learning and then switch to the task of stabilizing the system. The performance of the unstable and stable Koopman operators is shown in Fig. 7 for three different choices of prediction horizon. In cases where the system remains unstable, the states diverge and that biases the mean. For this reason, we compare the median score (in log scale) of the two approaches. In all cases, the stable Koopman operator stabilizes the dynamics. Further, it achieves a lower median than the unstable model.

## VI. DISCUSSION

This paper presents an algorithm for the computation of stable Koopman operators and introduces necessary conditions for the basis functions that are allowed, as well as conditions

for constructing Lyapunov functions for nonlinear dynamics. Further, it derives a formula for the global error (across arbitrary time steps into the future) induced by a Koopman operator, which motivates the use of stable operators in certain cases even when the underlying dynamics may not be stable.

We demonstrate the benefit of stable operators in the prediction and control of nonlinear dynamics and highlight its benefit in certain scenarios, such as in the low-sample limit which often arises in time-urgent tasks such as the one of stabilizing the dynamics of a quadrotor. Areas for future work include incorporating the stable operator with other inherent properties of the system, such as passivity.

## APPENDIX A EQUIVALENT MATRIX REPRESENTATION FOR SUM OF SQUARES ERROR

Note that the Frobenius norm of  $A \in \mathbb{R}^{m \times n}$  is

$$\|A\|_F = \sqrt{\sum_{i=1}^m \sum_{j=1}^n |a_{ij}|^2}.$$

Let  $\tilde{\mathcal{K}}_d \in \mathbb{R}^{W \times W}$  and  $\Psi(\cdot) \in \mathbb{R}^W$  and consider the expression

$$\sum_{k=1}^P \|\Psi(s_k(t_k + \Delta t), u_k(t_k + \Delta t)) - \tilde{\mathcal{K}}_d \Psi(s_k(t_k), u_k(t_k))\|^2. \quad (22)$$

Then, using the Frobenius norm definition for the vector  $\Psi(s_k(t_k + \Delta t), u_k(t_k + \Delta t)) - \tilde{\mathcal{K}}_d \Psi(s_k(t_k), u_k(t_k)) \in \mathbb{R}^W$ ,

$$(22) = \sum_{k=1}^P \left( \sum_{i=1}^W |\Psi_i(s_k(t_k + \Delta t), u_k(t_k + \Delta t)) - \tilde{\mathcal{K}}_{d_i} \Psi_i(s_k(t_k), u_k(t_k))|^2 \right)$$

where  $\tilde{\mathcal{K}}_{d_i} \in \mathbb{R}^W$  is a row vector that corresponds to the  $i$ th row of  $\tilde{\mathcal{K}}_d$ . Then, consider the term inside the absolute value

as the  $\mathcal{G}_{ik}$  element of a matrix  $\mathcal{G} \in \mathbb{R}^{W \times P}$  such that

$$(22) = \sum_{k=1}^P \left( \sum_{i=1}^W |\mathcal{G}_{ij}|^2 \right).$$

We can express  $\mathcal{G}$  as

$$\mathcal{G}^T = \begin{bmatrix} (\Psi(s_1(t_1 + \Delta t), u_1(t_1 + \Delta t)) - \tilde{\mathcal{K}}_d \Psi(s_1(t_1), u_1(t_1)))^T \\ \vdots \\ (\Psi(s_P(t_P + \Delta t), u_P(t_P + \Delta t)) - \tilde{\mathcal{K}}_d \Psi(s_P(t_P), u_P(t_P)))^T \end{bmatrix}$$

and rewrite it as

$$\begin{aligned} \mathcal{G}^T &= \begin{bmatrix} \Psi(s_1(t_1 + \Delta t), u_1(t_1 + \Delta t))^T \\ \vdots \\ \Psi(s_P(t_P + \Delta t), u_P(t_P + \Delta t))^T \end{bmatrix} \\ &- \begin{bmatrix} \Psi(s_1(t_1), u_1(t_1))^T \\ \vdots \\ \Psi(s_P(t_P), u_P(t_P))^T \end{bmatrix} \tilde{\mathcal{K}}_d^T. \end{aligned}$$

Let  $X, Y \in \mathbb{R}^{W \times P}$  such that

$$X = \begin{bmatrix} \Psi(s_1(t_1), u_1(t_1))^T \\ \vdots \\ \Psi(s_P(t_P), u_P(t_P))^T \end{bmatrix}^T$$

and

$$Y = \begin{bmatrix} \Psi(s_1(t_1 + \Delta t), u_1(t_1 + \Delta t))^T \\ \vdots \\ \Psi(s_P(t_P + \Delta t), u_P(t_P + \Delta t))^T \end{bmatrix}^T.$$

such that

$$\mathcal{G} = Y - \tilde{\mathcal{K}}_d X.$$

Then, using the Frobenius norm definition, we can rewrite (22) as

$$\begin{aligned} (22) &= \|\mathcal{G}\|_F^2 \\ &= \|Y - \tilde{\mathcal{K}}_d X\|_F^2. \end{aligned}$$

## APPENDIX B MEMORY PRESERVING GRADIENT DESCENTS

Consider  $\Psi(s(t)) \in \mathbb{R}^W$  and  $X, Y \in \mathbb{R}^{W \times P}$  such that

$$\Psi(s(t)) = [\Psi_1(s(t)) \ \Psi_2(s(t)) \ \dots \ \Psi_W(s(t))]^T$$

$$X = [\Psi(s(t_1)) \ \Psi(s(t_2)) \ \dots \ \Psi(s(t_P))]^T$$

and

$$Y = [\Psi(s(t_1 + \Delta t)) \ \Psi(s(t_2 + \Delta t)) \ \dots \ \Psi(s(t_P + \Delta t))]^T.$$

Then,

$$\begin{aligned} XX^T &= [\Psi(s(t_1)) \ \Psi(s(t_2)) \ \dots \ \Psi(s(t_P))] \begin{bmatrix} \Psi(s(t_1))^T \\ \Psi(s(t_2))^T \\ \vdots \\ \Psi(s(t_P))^T \end{bmatrix} \\ &= \begin{bmatrix} \Psi_1(s(t_1)) & \Psi_1(s(t_2)) & \dots & \Psi_1(s(t_P)) \\ \Psi_2(s(t_1)) & \Psi_2(s(t_2)) & \dots & \Psi_2(s(t_P)) \\ \vdots & \vdots & \dots & \vdots \\ \Psi_W(s(t_1)) & \Psi_W(s(t_2)) & \dots & \Psi_W(s(t_P)) \end{bmatrix} \\ &\cdot \begin{bmatrix} \Psi_1(s(t_1)) & \Psi_2(s(t_1)) & \dots & \Psi_W(s(t_1)) \\ \Psi_1(s(t_2)) & \Psi_2(s(t_2)) & \dots & \Psi_W(s(t_2)) \\ \vdots & \vdots & \dots & \vdots \\ \Psi_1(s(t_P)) & \Psi_2(s(t_P)) & \dots & \Psi_W(s(t_P)) \end{bmatrix} \\ &= \begin{bmatrix} \sum_{k=1}^P \Psi_1(s(t_k)) \Psi_1(s(t_k))^T & \dots & \sum_{k=1}^P \Psi_1(s(t_k)) \Psi_W(s(t_k))^T \\ \vdots & \ddots & \vdots \\ \sum_{k=1}^P \Psi_W(s(t_k)) \Psi_1(s(t_k))^T & \dots & \sum_{k=1}^P \Psi_W(s(t_k)) \Psi_W(s(t_k))^T \end{bmatrix} \\ &= \sum_{k=1}^P \begin{bmatrix} \Psi_1(s(t_k)) \Psi_1(s(t_k))^T & \dots & \Psi_1(s(t_k)) \Psi_W(s(t_k))^T \\ \vdots & \ddots & \vdots \\ \Psi_W(s(t_k)) \Psi_1(s(t_k))^T & \dots & \Psi_W(s(t_k)) \Psi_W(s(t_k))^T \end{bmatrix} \\ &= \sum_{k=1}^P \Psi(s(t_k)) \Psi(s(t_k))^T \\ &= \mathcal{G}. \end{aligned}$$

Similarly,  $YX^T = \mathcal{A}$ .

## REFERENCES

- [1] I. Abraham, G. De La Torre, and T. D. Murphey, “Model-based control using koopman operators,” *Proceedings of Robotics: Science and Systems*, 2017.
- [2] D. Bruder, B. Gillespie, C. D. Remy, and R. Vasudevan, “Modeling and control of soft robots using the Koopman operator and model predictive control,” in *Proceedings of Robotics: Science and Systems*, 2019.
- [3] M. T. Gillespie, C. M. Best, E. C. Townsend, D. Wingate, and M. D. Killpack, “Learning nonlinear dynamic models of soft robots for model predictive control with neural networks,” in *2018 IEEE International Conference on Soft Robotics (RoboSoft)*. IEEE, 2018, pp. 39–45.
- [4] B. Klaassen, R. Linnemann, D. Spenneberg, and F. Kirchner, “Biomimetic walking robot scorpion: Control and modeling,” *Robotics and autonomous systems*, vol. 41, no. 2-3, pp. 69–76, 2002.
- [5] Y. F. Zheng, H. Wang, S. Li, Y. Liu, D. Orin, K. Sohn, Y. Jun, and P. Oh, “Humanoid robots walking on grass, sands and rocks,” in *2013 IEEE Conference on Technologies for Practical Robot Applications (TePRA)*. IEEE, 2013, pp. 1–6.
- [6] G. Kan-feng and Z. Ming-yang, “Dynamic modeling and simulation of driving control for wheeled mobile robot on sand,” *Journal of System Simulation*, vol. 20, no. 18, pp. 5035–5039, 2008.
- [7] J. C. Kinsey, R. M. Eustice, and L. L. Whitcomb, “A survey of underwater vehicle navigation: Recent advances and new challenges,” in *IFAC Conference of Manoeuvering and Control of Marine Craft*, vol. 88, 2006, pp. 1–12.
- [8] G. Mamakoukas, M. A. MacIver, and T. D. Murphey, “Feedback synthesis for underactuated systems using sequential second-order needle variations,” *The International Journal of Robotics Research*, vol. 37, no. 13-14, pp. 1826–1853, 2018.
- [9] J. Yuh, “Modeling and control of underwater robotic vehicles,” *IEEE Transactions on Systems, man, and Cybernetics*, vol. 20, no. 6, pp. 1475–1483, 1990.

[10] G. Mamakoukas, M. A. MacIver, and T. D. Murphey, "Sequential action control for models of underactuated underwater vehicles in a planar ideal fluid," in *2016 American Control Conference (ACC)*. IEEE, 2016, pp. 4500–4506.

[11] S. L. Brunton, J. L. Proctor, and J. N. Kutz, "Discovering governing equations from data by sparse identification of nonlinear dynamical systems," *Proceedings of the National Academy of Sciences*, vol. 113, no. 15, pp. 3932–3937, 2016.

[12] W. Yu, J. Tan, C. K. Liu, and G. Turk, "Preparing for the unknown: Learning a universal policy with online system identification," *arXiv preprint arXiv:1702.02453*, 2017.

[13] O. Ennasr, G. Mamakoukas, M. Castaño, D. Coleman, T. Murphey, and X. Tan, "Adaptive single action control policies for linearly parameterized systems," in *ASME 2019 Dynamic Systems and Control Conference*. American Society of Mechanical Engineers Digital Collection, 2019.

[14] R. Johansson, A. Robertsson, K. Nilsson, and M. Verhaegen, "State-space system identification of robot manipulator dynamics," *Mechatronics*, vol. 10, no. 3, pp. 403–418, 2000.

[15] J. Swevers, W. Verdonck, and J. De Schutter, "Dynamic model identification for industrial robots," *IEEE control systems magazine*, vol. 27, no. 5, pp. 58–71, 2007.

[16] W. He, W. Ge, Y. Li, Y.-J. Liu, C. Yang, and C. Sun, "Model identification and control design for a humanoid robot," *IEEE Transactions on Systems, Man, and Cybernetics: Systems*, vol. 47, no. 1, pp. 45–57, 2016.

[17] I. Abraham and T. D. Murphey, "Active learning of dynamics for data-driven control using koopman operators," *Transactions on Robotics*, vol. 35, no. 5, pp. 1071–1083, 2019.

[18] A. Baranes and P.-Y. Oudeyer, "Active learning of inverse models with intrinsically motivated goal exploration in robots," *Robotics and Autonomous Systems*, vol. 61, no. 1, pp. 49–73, 2013.

[19] N. Roy and A. McCallum, "Toward optimal active learning through monte carlo estimation of error reduction," *ICML, Williamstown*, pp. 441–448, 2001.

[20] C. Dima, M. Hebert, and A. Stentz, "Enabling learning from large datasets: Applying active learning to mobile robotics," in *IEEE International Conference on Robotics and Automation, 2004. Proceedings. ICRA'04*. 2004, vol. 1. IEEE, 2004, pp. 108–114.

[21] D. Mayne, *Nonlinear Model Predictive Control: Challenges and Opportunities*, F. Allgöwer and A. Zheng, Eds. Basel: Birkhäuser Basel, 2000, vol. 26.

[22] B. O. Koopman, "Hamiltonian systems and transformation in Hilbert space," *Proceedings of the National Academy of Sciences*, vol. 17, no. 5, pp. 315–318, 1931.

[23] J. L. Proctor, S. L. Brunton, and J. N. Kutz, "Generalizing Koopman theory to allow for inputs and control," *SIAM Journal on Applied Dynamical Systems*, vol. 17, no. 1, pp. 909–930, 2018.

[24] I. Mezić, "On applications of the spectral theory of the Koopman operator in dynamical systems and control theory," in *Proceedings of the Conference on Decision and Control*, 2015, pp. 7034–7041.

[25] M. Budišić, R. Mohr, and I. Mezić, "Applied Koopmanism," *Chaos*, vol. 22, no. 4, p. 047510, 2012.

[26] M. Korda and I. Mezić, "Linear predictors for nonlinear dynamical systems: Koopman operator meets model predictive control," *Automatica*, vol. 93, pp. 149–160, 2018.

[27] A. Mauroy and J. Goncalves, "Linear identification of nonlinear systems: A lifting technique based on the Koopman operator," in *Proceedings of the Conference on Decision and Control*, 2016, pp. 6500–6505.

[28] S. L. Brunton, B. W. Brunton, J. L. Proctor, and J. N. Kutz, "Koopman invariant subspaces and finite linear representations of nonlinear dynamical systems for control," *PloS One*, vol. 11, no. 2, p. e0150171, 2016.

[29] E. Kaiser, J. N. Kutz, and S. L. Brunton, "Data-driven discovery of Koopman eigenfunctions for control," <https://arxiv.org/pdf/1707.01146.pdf>, 2017.

[30] N. Takeishi, Y. Kawahara, and T. Yairi, "Learning Koopman invariant subspaces for dynamic mode decomposition," in *Proceedings of the Neural Information Processing Systems*, 2017, pp. 1130–1140.

[31] M. Haseli and J. Cortés, "Efficient identification of linear evolutions in nonlinear vector fields: Koopman Invariant Subspaces," *arXiv preprint arXiv:1909.01419*, 2019.

[32] P. J. Schmid, "Dynamic mode decomposition of numerical and experimental data," *Journal of fluid mechanics*, vol. 656, pp. 5–28, 2010.

[33] M. O. Williams, I. G. Kevrekidis, and C. W. Rowley, "A data-driven approximation of the Koopman operator: Extending dynamic mode decomposition," *Journal of Nonlinear Science*, vol. 25, no. 6, pp. 1307–1346, 2015.

[34] C. Folkestad, D. Pastor, I. Mezic, R. Mohr, M. Fonoferova, and J. Burdick, "Extended dynamic mode decomposition with learned koopman eigenfunctions for prediction and control," *arXiv preprint arXiv:1911.08751*, 2019.

[35] H. Arbabi and I. Mezic, "Ergodic theory, dynamic mode decomposition, and computation of spectral properties of the koopman operator," *SIAM Journal on Applied Dynamical Systems*, vol. 16, no. 4, pp. 2096–2126, 2017.

[36] G. Mamakoukas, M. L. Castaño, X. Tan, and T. D. Murphey, "Local Koopman operators for data-driven control of robotic systems," in *Proceedings of Robotics: Science and Systems*, 2019.

[37] A. Mauroy and J. Goncalves, "Koopman-based lifting techniques for nonlinear systems identification," *arXiv preprint arXiv:1709.02003*, 2017.

[38] M. L. Castaño, A. Hess, G. Mamakoukas, T. Gao, T. Murphey, and X. Tan, "Control-oriented modeling of soft robotic swimmer with koopman operators," in *International Conference on Advanced Intelligent Mechatronics (AIM)*, 2020.

[39] A. M. Boudali, P. J. Sinclair, R. Smith, and I. R. Manchester, "Human locomotion analysis: Identifying a dynamic mapping between upper and lower limb joints using the koopman operator," in *2017 39th Annual International Conference of the IEEE Engineering in Medicine and Biology Society (EMBC)*. IEEE, 2017, pp. 1889–1892.

[40] B. W. Brunton, L. A. Johnson, J. G. Ojemann, and J. N. Kutz, "Extracting spatial-temporal coherent patterns in large-scale neural recordings using dynamic mode decomposition," *Journal of neuroscience methods*, vol. 258, pp. 1–15, 2016.

[41] I. Mezić, "Analysis of fluid flows via spectral properties of the koopman operator," *Annual Review of Fluid Mechanics*, vol. 45, pp. 357–378, 2013.

[42] J. Hogg, M. Fonoferova, and I. Mezic, "Exponentially decaying modes and long-term prediction of sea ice concentration using koopman mode decomposition," *arXiv preprint arXiv:1911.01450*, 2019.

[43] C. Folkestad, D. Pastor, I. Mezic, R. Mohr, M. Fonoferova, and J. Burdick, "Extended dynamic mode decomposition with learned koopman eigenfunctions for prediction and control," *arXiv preprint arXiv:1911.08751*, 2019.

[44] S. Sinha, B. Huang, and U. Vaidya, "Robust approximation of koopman operator and prediction in random dynamical systems," in *2018 Annual American Control Conference (ACC)*. IEEE, 2018, pp. 5491–5496.

[45] S. Sinha, U. Vaidya, and E. Yeung, "On computation of koopman operator from sparse data," in *2019 American Control Conference (ACC)*. IEEE, 2019, pp. 5519–5524.

[46] S. Sinha, H. Bowen, and U. Vaidya, "On robust computation of koopman operator and prediction in random dynamical systems," *arXiv preprint arXiv:1803.08562*, 2018.

[47] H. Lu and D. M. Tartakovsky, "Predictive accuracy of dynamic mode decomposition," *arXiv preprint arXiv:1905.01587*, 2019.

[48] B. Lusch, J. N. Kutz, and S. L. Brunton, "Deep learning for universal linear embeddings of nonlinear dynamics," *Nature Communications*, vol. 9, no. 1, p. 4950, 2018.

[49] K. Hara, M. Inoue, and N. Sebe, "Learning koopman operator under dissipativity constraints," *arXiv preprint arXiv:1911.03884*, 2019.

[50] D. Bruder, C. D. Remy, and R. Vasudevan, "Nonlinear system identification of soft robot dynamics using koopman operator theory," in *2019 International Conference on Robotics and Automation (ICRA)*. IEEE, 2019, pp. 6244–6250.

[51] R. Tibshirani, "Regression shrinkage and selection via the lasso," *Journal of the Royal Statistical Society: Series B (Methodological)*, vol. 58, no. 1, pp. 267–288, 1996.

[52] P. J. Antsaklis and A. N. Michel, *Linear systems*. Springer Science & Business Media, 2006.

[53] D. A. Dowler, "Bounding the norm of matrix powers," 2013.

[54] J. Leader, "The norms of powers of matrices with unit spectral radius," *Applied Mathematics Letters*, vol. 7, no. 2, pp. 15–17, 1994.

[55] N. J. Higham and P. A. Knight, "Matrix powers in finite precision arithmetic," *SIAM journal on matrix analysis and applications*, vol. 16, no. 2, pp. 343–358, 1995.

[56] N. Gillis, M. Karow, and P. Sharma, "Approximating the nearest stable discrete-time system," *Linear Algebra and its Applications*, vol. 573, pp. 37–53, 2019.

[57] N. Borovykh and M. Spijker, "Resolvent conditions and bounds on the powers of matrices, with relevance to numerical stability of initial value problems," *Journal of Computational and Applied Mathematics*, vol. 125, no. 1-2, pp. 41–56, 2000.

- [58] G. Halikias, L. Dritsas, A. Pantelous, and V. Tsoukas, "Strong stability of discrete-time systems," *Linear Algebra and its Applications*, vol. 436, no. 7, pp. 1890–1908, 2012.
- [59] P. Shcherbakov, "On peak effects in discrete time linear systems," in *2017 25th Mediterranean Conference on Control and Automation (MED)*. IEEE, 2017, pp. 376–381.
- [60] U. Ahiyevich, S. E. Parsegov, and P. S. Shcherbakov, "Upper bounds on peaks in discrete-time linear systems," *Automation and Remote Control*, vol. 79, no. 11, pp. 1976–1988, 2018.
- [61] T. A. Berrueta, A. Pervan, K. Fitzsimons, and T. D. Murphey, "Dynamical system segmentation for information measures in motion," *IEEE Robotics and Automation Letters*, vol. 4, no. 1, pp. 169–176, 2018.
- [62] B. Boots, G. J. Gordon, and S. M. Siddiqi, "A constraint generation approach to learning stable linear dynamical systems," in *Advances in neural information processing systems*, 2008, pp. 1329–1336.